

Toluene and naphthalene sorption by iron oxide/clay composites

Part I. Materials characterization

Marilda M. G. R. Vianna · Jo Dweck ·
Frank H. Quina · Flavio M. S. Carvalho ·
Claudio A. O. Nascimento

Received: 14 April 2009 / Accepted: 17 August 2009 / Published online: 10 September 2009
© Akadémiai Kiadó, Budapest, Hungary 2009

Abstract Commercial bentonite (BFN) and organoclay (WS35), as well as iron oxide/clay composite (Mag_BFN) and iron/oxide organoclay composite (Mag_S35) were prepared for toluene and naphthalene sorption. Mag_BFN and Mag_S35 were obtained, respectively, by the precipitation of iron oxide hydrates onto sodium BFN and S35 clay particles. The materials were characterized by powder X-ray diffraction (XRD), X-ray Fluorescence (XRF), and TG and DTA. From XRF results and TG data on calcined mass basis, a quantitative method was developed to estimate the iron compound contents of the composites, as well as the organic matter content present in WS35 and Mag_S35.

Keywords Clay · Organoclay · Iron oxide/clay composites · Characterization · Thermal analysis

Abbreviations

BFN	Commercial bentonite
BTEX	Benzene, toluene, ethylbenzene, and xylenes
d_{001}	Basal spacing

M. M. G. R. Vianna (✉) · C. A. O. Nascimento
Chemical Engineering Department, Polytechnic School,
University of São Paulo, São Paulo, SP, Brazil
e-mail: marilda@pqi.ep.usp.br

J. Dweck
School of Chemistry, Rio de Janeiro Federal University, Rio de Janeiro, RJ, Brazil

F. H. Quina
Chemical Institute, University of São Paulo, São Paulo, SP, Brazil

F. M. S. Carvalho
Geosciences Institute, University of São Paulo, São Paulo, SP, Brazil

DTA	Differential thermal analysis
Mag_BFN	Iron oxide/clay composite
Mag_S35	Iron/oxide organoclay composite
M_{CS}	Calcined mass of sample S
M_{IS}	Initial mass of sample S
NOC	Nonpolar organic compounds
PAH	Polycyclic aromatic hydrocarbons
S35	Unwashed organoclays
TG	Thermogravimetry
WS35	Washed organoclay
XRD	Powder X-ray diffraction (XRD)
XRF	X-ray fluorescence
$\gamma\text{-Fe}_2\text{O}_3$	Maghemite

Introduction

Clay minerals, especially smectites, have long attracted attention for their wide scale application in industry and are used in the construction of liners for hazardous waste landfills, slurry walls, industrial waste treatment lagoons, sewage lagoons, and tank farms [1]. Bentonites are rocks that are composed dominantly of smectite. Smectite clays contain inorganic cations such as Na^+ and Ca^{2+} that are strongly hydrated in the presence of water, promoting hydrophilic properties to the clay particles. When these inorganic cations are replaced by large organic cations of the form $[(\text{CH}_3)_3\text{NR}]^+$ or $[(\text{CH}_3)_2\text{NR}_2]^+$, where R is a large (C_{12} or greater) alkyl hydrocarbon, these change the clay characteristics from hydrophilic to organophilic. This exchange results in an organoclay with physical and chemical properties that are different from those of unmodified clay [2]. Organoclays are effective sorbents for a wide number of aqueous nonpolar organic compounds (NOCs). In contrast, inorganic bentonites show very weak

sorptive capabilities for these compounds [3]. Benzene, toluene, ethylbenzene, and xylenes (BTEX), are the standard contaminants in groundwater contaminated by leakage from underground gasoline storage tanks. Polycyclic aromatic hydrocarbons (PAHs), with two or more fused benzene rings, are ubiquitous environmental contaminants. Applications of organoclays in pollution prevention as sorbents for NOCs from aqueous solutions include the treatment of waste effluents, as extenders for activated carbon and as components of clay barriers around waste disposal reservoirs and oil or gasoline tanks [3–5].

Other kinds of clays are the clay-nanocrystalline composites, obtained by the allocation of nanophase particles onto the clay surfaces, which may be semiconductors [6, 7], magnetic particles [8–10], and metallic particles [11]. Clays modified with magnetic particles are promising materials for many important uses such as biochemical [12], technological, environmental, and industrial applications [8–10]. Magnetic adsorbents are an alternative to conventional sorbents and have the advantage that they can be separated from the surrounding medium by a simple magnetic process after their use [8].

Very often chemical or instrumental analysis techniques are used to quantify the chemical composition of the clays or modified clays other than thermal analysis techniques [13–15]. No study has been published so far about the quantification of the iron compounds present in iron oxide/organoclay composites by thermal analysis as presented in this article. In this first part of the study, we assess the characterization of a commercial natural bentonite (BFN), which was used as the raw material for the two synthetic organoclays (WS35 and S35), the iron oxide/clay composite (Mag_BFN) and iron/oxide organoclay composite (Mag_S35). These compounds were used as sorbents of toluene and naphthalene. The characterization of these materials was done by X-ray diffraction, thermogravimetry, differential thermal analysis, and X-ray fluorescence analysis. In the second part of the study, which is presented in Part II, we compare the capacities of clay (BFN), organoclay (WS35), iron oxide/clay (Mag_BFN), and iron oxide/organoclay composites (Mag_S35) to remove organic compounds from water by sorption. Toluene was used as a solute model to represent BTEX compounds, since it exhibits intermediate physical and chemical characteristics of the other BTEX compounds, and naphthalene was chosen to represent PAH compounds.

Materials and methods

The natural bentonite (BFN) and the organoclays (S35 and WS35), supplied by the industry BF-Clay Especialidades Ltda, São Paulo, SP, Brazil, were used to obtain the iron

oxide composites. BFN bentonite has Na^+ as the primary exchangeable cation and a cation exchange capacity (CEC) of 110 cmol/kg. S35 is the commercial organophilic clay obtained from BFN, by cation exchange with dimethylditallowammonium chloride (DMDTA Cl). After it has been washed and dried at 60 °C, WS35 organoclay was obtained. The other raw materials, NaOH , FeCl_3 , and $\text{FeSO}_4 \cdot 7\text{H}_2\text{O}$, supplied by Vetec Química Fina Ltda., Duque de Caxias, RJ, Brazil, were used as received. The chemical composition of the clays and iron oxide composites is shown in Table 2 of next item. Details of the preparation of the iron oxide/clay composites have been reported previously [8]. Briefly, iron oxide hydrates were precipitated in situ by drop wise addition of NaOH into a solution of the iron salts, where BFN clay or S35 organoclay were added prior to the reaction with NaOH . The iron oxide composites were dialyzed with distilled water until free of residual Cl^- ions, tested by AgNO_3 . The wet clay composite (Mag_BFN) or organoclay composite (Mag_S35) phases were dried at 60 °C and then mechanically milled until 100% passed through a 200-mesh sieve.

Basal spacings were determined by X-ray diffraction (XRD) analysis using $\text{Cu K}\alpha$ radiation ($\lambda = 0.15416 \text{ nm}$) and a Siemens Model D5000 X-ray diffractometer, by using $0.02^\circ 2\theta$ steps at 1.0 s/step. The data were analyzed by Diffraction Plus software, integrated with Jcpds- International Center for Diffraction Data (ICDD) version 2001, PDF 2. Chemical compositions were determined by X-ray fluorescence by using Phillips Spectrometer model PW 2404 XRF.

Simultaneous Thermogravimetric (TG) and Differential Thermal Analysis (DTA) were performed in platinum pans in a TA Instruments, model SDT2960 equipment, by using 100 mL min^{-1} air flow, from 28 to 1,000 °C with a 10 °C/min heating rate. Alpha-alumina was used as reference for DTA measurements. Derivative Thermogravimetric curves (DTG) were obtained by using the data analysis software of the instrument.

Results and discussion

X-ray diffraction

Figures 1 and 2 show the XRD patterns of BFN, S35, WS35, Mag_BFN, and Mag_S35 samples and Table 1, the respective interlayer spacing values. The raw material, BFN bentonite (Fig. 1a), consists of Na-smectite with minor amounts of quartz and feldspar. 1.56 nm basal spacing indicates the presence of smectite. A small reflection at 0.15 nm indicates the presence of dioctahedral mineral. The reflections at 0.34 and 0.32 nm are due to quartz and feldspar impurities, respectively. S35 sample

(Fig. 1b) was not dialyzed because it was used as the raw material for preparation of Mag_S35. The X-ray diffraction pattern of S35 sample shows two reflections at 1.94 and 1.26 nm. These indicate that it is interstratified, as does the reflection at 3.20 nm. Two orders of the interlayer spacing (d_{001}) are also observed for WS35 (Fig. 2a) (2.68 and 1.26 nm), which is also interstratified. Evidence for interstratification of the organic layer (2.68 nm) with a Na^+ interlayer (1.26 nm) has been reported for clays partially exchanged with HDTMA [4]. Basal space in this case would necessarily reflect the interlayer spacing exclusively occupied by each cation. The XRD patterns obtained for S35 and WS35 (Figs. 1b and 2a, respectively) are significantly different: WS35 presents a larger basal spacing (2.68 nm) than S35 (1.94 nm). The positions of the basal reflections vary according to the separation of the structural layers (the interlayer spacing), which is influenced by the exchanged cation and its exchange degree, as occurs for example during S35 washing, leading to a higher WS35 basal spacing. The physical arrangement of the organic cation within interlayers is changed. Based on the d_{001} spacings shown in Figs. 1b and 2a and to Lagaly [16] and Jaynes and Boyd [17] results, the S35 and WS35

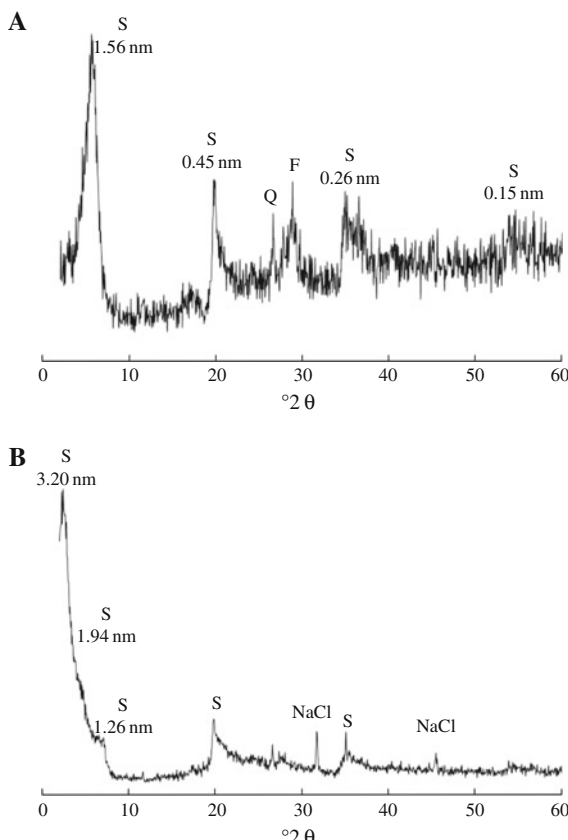


Fig. 1 XRD patterns for **a** the pure bentonite BFN; **b** the organoclay S35. *S* smectite, *Q* quartz, *F* feldspar

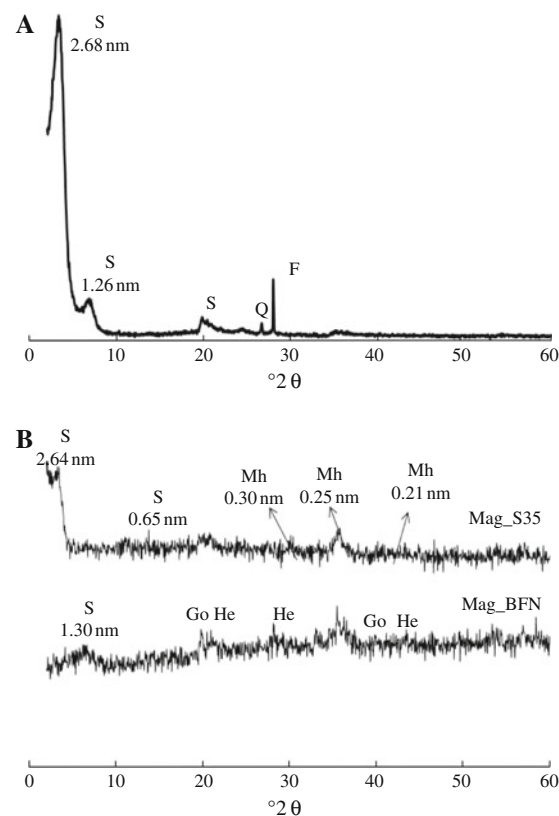


Fig. 2 XRD for the **a** WS35 and **b** clay/iron oxide composites Mag_S35 and Mag_BFN. *S* smectite, *Mh* maghemite *Go* goethite, *He* hematite

Table 1 Interlayer spacing of the materials

Samples	Interlayer spacing d_{001}/nm
BFN	1.56
Mag_BFN	1.30
S35	1.94
WS35	2.68
Mag_S35	2.64

organoclays have, respectively, a pseudotrimolecular and paraffin layer complex within their structure.

The X-ray diffraction patterns of Mag_S35 and Mag_BFN are presented in Fig. 2b. The most intense low-angle reflections at 2.64 and 1.30 nm correspond to the d_{001} basal spacing of the Mag_S35 and Mag_BFN samples, respectively. The S35 reflection at 1.94 nm (Fig. 1b) was shifted to 2.64 nm in Mag_S35. The values of the d_{001} -spacings of WS35 (Fig. 2a) and Mag_S35 (Fig. 2b) are practically the same (2.68 and 2.64 nm), so the addition of iron did not change the basal spacing of the Mag_S35. Assuming a layer thickness in smectite of 0.96 nm, an interlayer distance of 1.72–1.68 nm can be estimated. As presented in Fig. 1, the results showed a significant

increase of the basal spacing from 1.56 in BFN case, 2.68–2.64 nm in WS35, and Mag_S35 cases, respectively. These samples yielded values of d_{001} consistent with paraffin complexes [16]. In both XRD patterns shown in Fig. 1d, there are higher order reflections at $d_{001} = 0.65, 0.30, 0.25$, and 0.21 nm that can be related to the presence of maghemite (ICDD 39-1346). Weak diffraction peaks are also observed, which might be related to the presence of goethite (ICDD 29-0713) and hematite (ICDD 33-0664). This suggests that the main iron oxide phase present is maghemite ($\gamma\text{-Fe}_2\text{O}_3$), similar to the clay/iron oxide composites prepared by Oliveira et al. [8].

Chemical composition by XRF

Table 2 presents the chemical composition of BFN, Mag_BFN, S35, WS35, and Mag_S35 samples obtained from X-ray Fluorescence analysis. Practically in all the cases, the inorganic oxides of the original clay matrix of a sample are present in the calcined mass after ignition (Mc), which is the sum of all present oxide masses. From the same mass of BFN, a same SiO_2 mass is present on

corresponding masses formed of all other studied compounds. Thus, Table 3 presents Table 2 on silicon oxide basis to have a same basis of comparison to analyze the different samples. The Fe_2O_3 contents of Mag_BFN and Mag_S35 are higher than those of the clays used to obtain them due to the iron compounds added during each formation process. The same occurs to Mn and Ca contents of Mag_BFN and Mag_S35, expressed in respective oxide contents, caused probably by the presence of these elements as impurities of the iron salts used to produce the composites. The sodium contents of WS35 and Mag_S35 are much lower than in S35, which, as confirmed in Fig. 1b, still contains the sodium salt (NaCl) formed during its formation process, which in turn is extracted by the liquid aqueous phase during WS35 and Mag_S35 obtention processes.

In Table 4 are shown, on SiO_2 mass basis, the Fe_2O_3 contents due to the original clay and to the iron compounds of the clay coating, formed from respective iron salt precursors by reaction with sodium hydroxide.

In order to prepare the composites, the iron salts were added at the same mass ratio to BFN and S35. As in

Table 2 Chemical compositions from X-ray Fluorescence (XRF) analysis

Sample	SiO_2	Al_2O_3	MnO	MgO	CaO	Na_2O	K_2O	TiO_2	P_2O_5	Fe_2O_3	LOI
BFN	61.67	19.28	0.04	3.09	1.07	2.71	0.36	0.22	0.05	4.59	5.94
Mag_BFN	34.60	10.82	0.20	1.81	0.70	1.50	0.13	0.13	0.02	42.87	6.97
S35	43.40	13.60	0.03	2.27	0.71	2.32	0.24	0.16	0.04	3.15	35.10
WS35	44.20	13.80	0.04	2.19	0.43	0.24	0.23	0.16	0.04	3.22	36.0
Mag_S35	21.61	7.11	0.22	1.21	1.18	0.17	0.10	0.08	0.02	44.89	22.26

Table 3 Chemical compositions on silicon oxide basis

Sample	SiO_2	Al_2O_3	MnO	MgO	CaO	Na_2O	K_2O	TiO_2	P_2O_5	Fe_2O_3	Mc
BFN	100	31.26	0.06	5.01	1.74	4.39	0.58	0.36	0.08	7.44	150.93
Mag_BFN	100	31.27	0.58	5.23	2.02	4.34	0.38	0.38	0.06	123.90	268.15
S35	100	31.34	0.07	5.23	1.64	5.35	0.55	0.37	0.09	7.26	151.89
WS35	100	31.22	0.09	4.95	0.97	0.54	0.52	0.36	0.09	7.29	146.04
Mag_S35	100	32.90	1.02	5.60	5.46	0.79	0.46	0.46	0.09	207.73	354.51

Table 4 Other composition data on silicon oxide basis and ratios between calcined masses

Sample	Clay Fe_2O_3	Coating Fe_2O_3	Other oxides	$M_c\text{BFN}/M_c\text{S}$	$M_c\text{WS35}/M_c\text{S}$	$M_c\text{S35}/M_c\text{S}$
BFN	7.44	0.00	143.49	1.0000	0.9676	1.0063
Mag_BFN	7.44	116.46	144.25	0.5629	0.5446	0.5664
S35	7.26	0.00	144.63	0.9937	0.9615	1.0000
WS35	7.29	0.00	138.76	1.0335	1.0000	1.0400
Mag_S35	7.29	200.44	146.78	0.4257	0.4112	0.4285

* M_c sample calcined mass from Table 3

Mag_S35 case, the SiO_2 content of the organophilic clay is lesser than in BFN case, it can be seen from Table 4 that, with respect to the SiO_2 content of the ceramic matrix of each case, the relative added Fe_2O_3 content of Mag_S35 is much higher than that of Mag_BFN.

Thermal analysis

Figure 3 shows the TG, DTG, and DTA curves of BFN and Mag_BFN samples. The former presents a total of 6.74% free and adsorbed water, which is lost in two steps up to 150 °C [15]. The latter exhibits a lower water loss (5.65%), which ends at the same temperature. From 160 to 307 °C, the resulting DTA is endothermic due to the dehydroxylation of hydrated iron oxides.

The thermal dehydroxylation reaction of these hydrated phases, which have structural OH, may take place at widely varying temperatures (140–500 °C) depending on the nature of the compound [18]. The structural dehydroxylation of Mag_BFN occurs from 500 to 720 °C, at the same

temperature range than that of the original clay (BFN), as seen from DTG curves.

When initial compositions of samples are different, thermal analysis curve data based on respective initial masses, as shown in Fig. 3, can not be used to directly compare the contents of their main phases or to compare TG mass losses or DTA peak thermal effects. However, considering that: (a) the ignited calcined mass of a sample S, used to obtain its chemical composition by XRF has the same oxide composition than that of the calcined mass residue at 1,000 °C of respective TG curve (M_{cS}) and (b) the ratio between the calcined masses of the samples may be calculated on a same oxide basis as shown on Table 4 (silicium oxide in the present case), non conventional procedures based on the ratio between calcined masses may be used for a correct comparative quantitative analysis.

The ratio between initial and calcined mass of a sample in a TG curve is the same, independently of the basis on which the curve was plotted (initial mass basis or other one). Thus, if two samples have different initial mass compositions, but the ratio between their respective calcined masses is known, (in the present cases, from Table 4), TG and DTG curves of a sample can be plotted on the basis of the initial mass of the other one, to have a same basis of comparison and calculation, as follows.

S35 and BFN characterization

From the original TG plots, based on respective initial mass basis, $M_{cS35} = 62.43\%$ and $M_{cBFN} = 88.04\%$. From Table 4, M_{cBFN} represents 99.37% of M_{cS35} . Figure 4 shows BFN and S35 TG and DTG curves, which were plotted on a same S35 initial mass basis (M_{iS35}), to compare on a same basis, the mass losses of each case, and to estimate the content of the organic matter of S35. This was

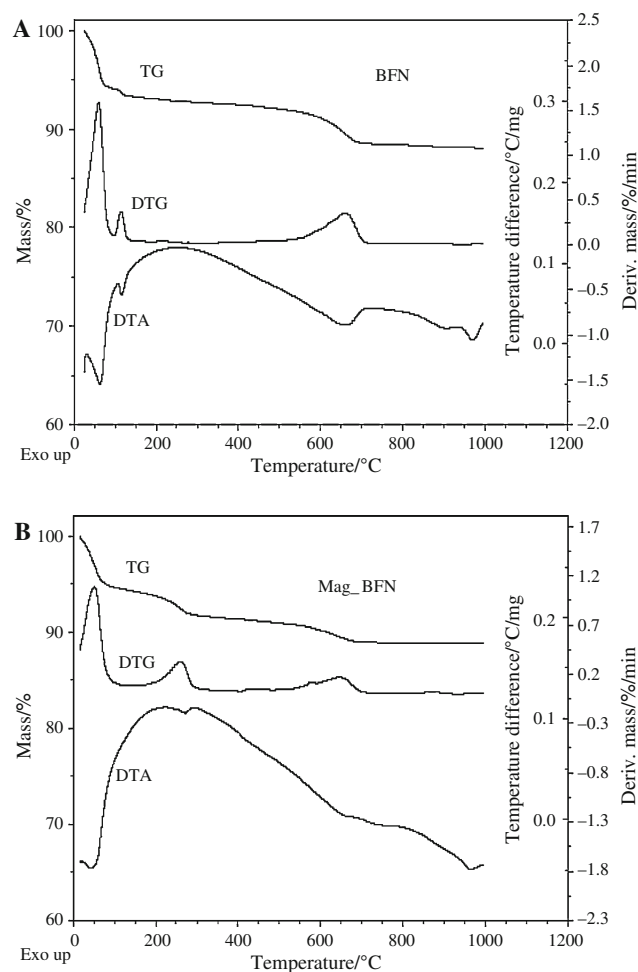


Fig. 3 TG, DTG, and DTA curves of BFN (a) and Mag_BFN (b)

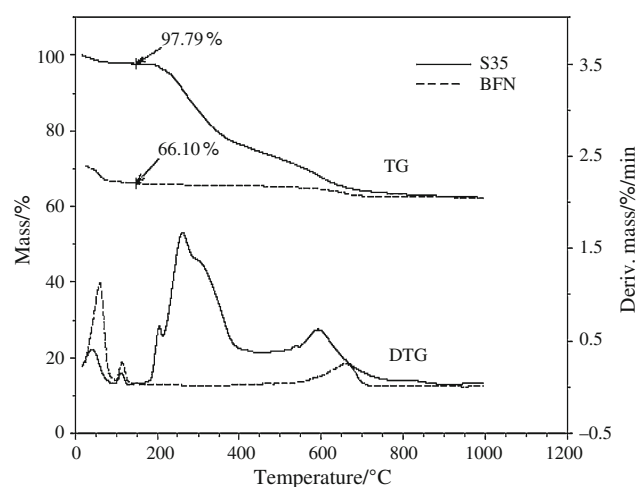


Fig. 4 BFN and S35 TG and DTG curves on S35 initial mass basis

done by using the data analysis software of the equipment to multiply all the points of the TG and DTG curves of BFN sample on initial mass basis (shown on Fig. 3a) by $(0.9937 \times 62.40/88.04)$.

From Fig. 4, it can be seen that dried masses of S35 and BFN samples are, respectively, equal to 97.79 and 66.10% of M_{iS35} and the calcined masses of these samples are, respectively, equal to 62.43 and 62.04% of M_{iS35} . From S35 dried condition to its final calcined condition, the mass loss during analysis is due to the water lost from structural dehydroxylation plus the loss of the respective organic content, which is burnout during analysis. As on the same M_{iS35} basis, the S35 dehydroxylation mass loss is equal to BFN dehydroxylation mass loss, which is equal to $(66.10 - 62.04) = 4.06\%$ of M_{iS35} , the organic content of S35 is equal to $(97.79 - 62.43 - 4.06) \times 100/97.79 = 32.01\%$ of its dried mass.

The dehydroxylation of S35 organoclay occurs at a lower temperature than BFN matrix dehydroxylation because of its higher interlayer space, and the thermal energy released during organics combustion [3, 19].

WS35 characterization

From Table 4, WS35 calcined mass is equal to 96.15% of S35 calcined mass. In order to have a same basis of comparison, Fig. 5 shows their TG, DTG, and DTA curves on S35 initial mass basis, obtained in a similar procedure than in the previous case. As can be seen, they present initially the loss of free and/or sorbed water, characterized by the respective endothermic DTA peaks, below 130 °C. From 150 to 210 °C, the organic matter of the S35 sample began to be released as indicated by respective DTG peak. From the respective sharp exothermic DTA peak within this temperature range, it can be seen that combustion also

occurs. From this temperature to 400 °C, as shown from S35 TG curves, a higher organic release occurred due to continuous pyrolysis and combustion steps and a lower residual mass remained to be burned during the final combustion step [20].

The initial pyrolysis behavior can probably be explained by the fact that S35 organoclay still contains residual weakly adsorbed organic cation and/or original quaternary salt on the external surface of its particles. Note that during S35 washing, its basal space increases from 1.94 to 2.68 nm, which indicates a higher organic cation content in the interlayer space of WS35 than in S35. As no additional QUAT was added during washing, this increase in interlayer organic cation content could only be supplied from the external surface of the particle.

A second evidence of the previous fact is that, as seen from DTG curves of the WS35 clay, the organics pyrolysis begins practically at 200 °C, showing a higher thermal stability than the organics of the S35 organoclay [3], which may be explained to a higher bonding force with the interlayer structure. From this temperature to 400 °C, the resulting DTA effect is exothermic, due to the burnout of the organic matter. In both cases, dehydroxylation of clay structure occurs between 500 and 720 °C identified by respective DTG peak, practically within the same range as original clay, as shown in Fig. 5 simultaneously to organics burnout. After this step, the residual carbonaceous material burns out [3], characterized by a small and broad exothermal DTA peak. Note that the DTG peaks begin at lower temperatures than the corresponding DTA peaks, indicating that combustion occurred after pyrolysis had begun [15]. It must be noted that S35 presents a much lower combustion of residual carbonaceous matter than WS35 from 720 to 800 °C because it has less organic matter within its interlayer space.

From Figs. 4 and 5, which are plotted on a same M_{iS35} basis, it can be seen that dried masses of WS35 and BFN samples are, respectively, equal to 94.03 and 66.10% and calcined masses of these samples are, respectively, equal to 60.01 and 62.04% of M_{iS35} . As occurred in S35 case, from the WS35 dried condition to its final calcined condition the mass loss is due to the water lost from its structural dehydroxylation plus the loss of all respective organic content. As on a same M_{iS35} basis, the WS35 dehydroxylation mass loss is also equal to the dehydroxylation mass loss of BFN, previously calculated as being equal to 4.06% of M_{iS35} , the WS35 organic matter content is equal to $(94.03 - 60.01 - 4.06) \times 100/94.03 = 31.86\%$ of its dried mass.

These results indicate that S35 and WS35 organoclays have, on dried basis, practically the same content of organics in their structure. This is an additional fact which confirms that, during S35 washing, the aqueous media enhances ion dissociation and diffusion and, consequently,

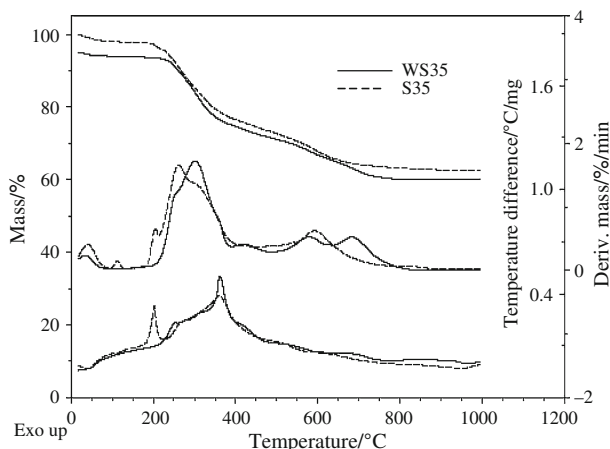


Fig. 5 TG, DTG, and DTA curves of S35 and WS35 on S35 initial mass basis

provides better conditions for additional cation exchange with previously existent salt adsorbed in external surface of S35 and/or for diffusion of externally adsorbed cations to the interlayer space of the resulting WS35 organoclay.

Mag_BFN composite characterization

From Fig. 3 TG curves, plotted on respective sample initial mass basis, $M_{c\text{BFN}} = 88.04\%$ and $M_{c\text{Mag_BFN}} = 88.78\%$. From Table 4, $M_{c\text{BFN}}$ represents 56.29% of $M_{c\text{Mag_BFN}}$. Figure 6 shows Mag_BFN and BFN TG and DTG curves, which were plotted on a same Mag_BFN initial mass basis ($M_{i\text{Mag_BFN}}$), to compare on a same basis, the mass losses of each case and to estimate the contents of the iron oxide compounds and BFN clay matrix of Mag_BFN. From Fig. 6, it can be seen that BFN dried mass represents $(52.96 \times 100/94.29) = 56.17\%$ of Mag_BFN dried mass. Thus, it can be estimated that the iron compounds content of Mag_BFN, on dried mass basis, is $(100 - 56.17) = 43.83\%$.

This same basis of comparison shows that Mag_BFN DTG curve does not present the dehydration peak of BFN observed between 100 and 150 °C. After respective drying, the main difference between composite and matrix DTG peaks is the loss of water from the dehydroxylation of the hydrated iron oxides present in Mag_BFN, characterized by a DTG peak from 150 to 400 °C. The dehydroxylation of respective ceramic matrix occurs from 500 to 750 °C, as shown from respective DTG peaks.

Mag_S35 composite characterization

From TG curves on respective initial mass basis, $M_{c\text{S35}} = 62.40\%$ and $M_{c\text{Mag_S35}} = 76.13\%$. From Table 4, $M_{c\text{WS35}}$ represents 42.85% of $M_{c\text{Mag_S35}}$. Figure 7 shows Mag_S35

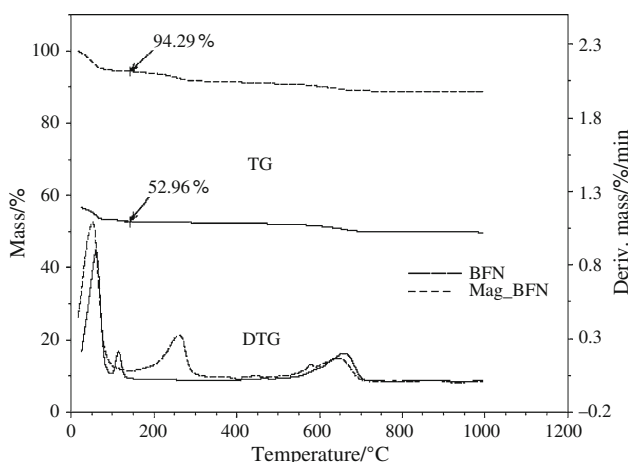


Fig. 6 BFN and Mag_BFN TG and DTG curves on Mag_BFN initial mass basis

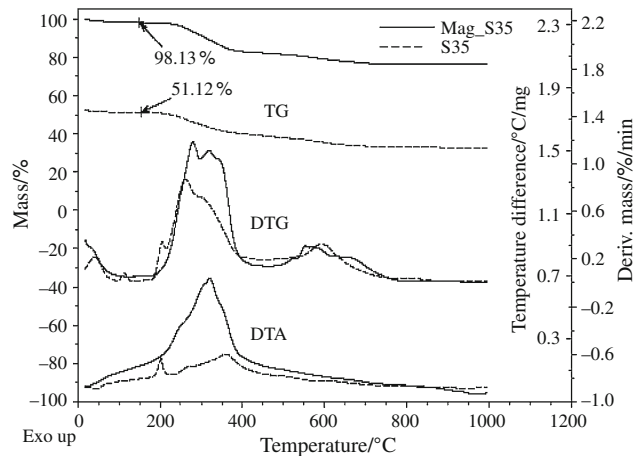


Fig. 7 Mag_S35 and S35 TG, DTG and DTA curves on Mag_S35 initial mass basis

and S35 TG DTG and DTA curves, which were plotted on a same Mag_S35 initial mass basis ($M_{i\text{Mag_BFN}}$), to compare on a same basis, the mass losses of each case and to estimate the contents of iron oxide compounds, organics, and clay matrix of Mag_S35 composite.

From Fig. 7, it can be seen that free and adsorbed water of Mag_35 are lost before 150 °C, the same drying temperature than Mag_BFN. From TG and DTG peaks, it can be seen that there are two main steps of mass loss. The first occurs from 150 to 450 °C, during which, organic content pyrolysis and burning occur simultaneously to the dehydroxylation of the present iron oxide hydrates. During the second step, from 450 to 800 °C, the clay structure dehydroxylation occurs with the simultaneous residual carbonaceous matter burnout. The DTA curve of Mag_S35, between 150 and 500 °C, presents a much higher and broader exothermic peak than the S35 DTA curve in the same temperature range. This much higher evolved energy and correspondent rate may probably be due to the simultaneous exothermic oxidation of ferrous oxide to ferric oxide with the exothermic combustion of the released organics, increasing the actual temperature of the sample, which in turn accelerates both reactions.

Figure 7 also shows that in the case of Mag_S35 composite, the organics mass loss begins at higher temperatures than in the case of S35 organophilic clay. This indicates that, the aqueous media promote a similar structural change to the one that occurred in the case the transformation from S35 to WS35, giving a higher thermal stability to the organics present in Mag_S35. As seen from XRD data, the values of basal spacing of WS35 and Mag_S35 are very similar.

From Fig. 7, it can be seen that S35 dried mass represents $(51.12 \times 100/98.13) = 52.09\%$ of Mag_S35 dried mass. Thus, it can be estimated that the content of iron oxide

compounds of Mag_S35, on its dried mass basis, is $(100 - 52.09) = 47.91\%$. From previous discussed characterization data, dried S35 has 32.01% of organic components, so a clay matrix composes the rest. Thus, it can be estimated that Mag_S35 has $(0.3201 \times 52.09) = 16.67\%$ of organic matter and $(52.09 - 16.67) = 35.42\%$ of clay matrix on dry basis.

Conclusions

- By using thermogravimetry on calcined mass basis and the respective oxide compositions obtained by XRF, the developed quantitative analysis method allows one to estimate the contents of the iron oxide compounds and of the clay matrix of the Mag_BFN and Mag_S35 composites, as well as their organic contents and those of the original S35 and modified WS35 organophilic clays.
- An increase of basal spacing (d_{001}) occurs when S35 is transformed to WS35 in aqueous suspension. As measured by quantitative thermal analysis, the organic matter contents of S35 and WS35 on dried basis are practically the same. Therefore, this increase indicates that during S35 washing, the aqueous media promote the organic matter to migrate from the outer surface of S35 particles to the interlayer space of the final WS35 clay structure.
- This is also confirmed by the higher thermal stability of WS35 when compared to S35, by the higher temperature needed to release the organic contents of the former, as shown by respective thermal analysis results.
- WS35 and Mag_S35 present d_{001} basal spacing values consistent with those of organophilic clays containing paraffin complexes.
- No change was observed in basal spacing (d_{001}) upon precipitation of the iron hydroxides onto the S35 to obtain Mag_S35 composite, indicating that the precipitation occurs on the external surfaces of the organophilic clay particles.
- This kind of precipitation is also confirmed by XRD patterns, through which, it can be seen that maghemite ($\gamma\text{-Fe}_2\text{O}_3$) is the main iron oxide phase present on the external surface of Mag_BFN and Mag_S35 particles, which confers their magnetic properties.

Acknowledgements To the National Institute of Science and Technology for Environmental Studies (INCT-EMA), State of São Paulo Research Foundation (FAPESP), BF Clay Especialidades Lta, X-ray Laboratory, and X-ray Fluorescence Laboratory of the Geosciences Institute of the University of São Paulo.

References

1. Jaynes WF, Boyd SA. Trimethylphenylammonium-smectite as an effective adsorbent of water soluble aromatic hydrocarbons. *J Air Waste Manag Assoc.* 1990;40:1649–53.
2. Yariv S, Lapides I. The use of thermo-xrd-analysis in the study of organo-smectite complexes. *J Therm Anal Calorim.* 2005;80: 11–26.
3. Vianna MMG, Dweck J, Kozievitch VJ, Valenzuela-Diaz FR, Büchler PM. Characterization and study of sorptive properties of differently prepared organoclays from a Brazilian natural bentonite. *J Therm Anal Calorim.* 2005;82:595–602.
4. Boyd SA, Mortland MM, Chiou CT. Sorption characteristics of organic compounds on hexadecyltrimethylammonium-smectite. *Soil Sci Soc Am J.* 1988;52:652–7.
5. Sora NI, Pelosato R, Zampori L, Botta D, Dotelli G, Vitelli M. Matrix optimization for hazardous organic waste sorption. *Appl Clay Sci.* 2005;28:43–54.
6. Dekany I, Turi L, Tombacz E, Fendler JH. Preparation of size-quantized CdS and ZnS particles in nanoparticle reactors provided by binary liquids adsorbed at layered silicates. *Langmuir.* 1995; 11:2285–92.
7. Dekany I, Turi L, Kiraly Z. CdS, TiO and Pd8 nanoparticles growing in the 2 interlamellar space of montmorillonite in binary liquids. *Appl Clay Sci.* 1999;15:221–39.
8. Oliveira LCA, Rios RVRA, Fabris JD, Lago RM. A simple preparation of magnetic composites for the adsorption of water contaminants. *J Chem Educ.* 2004;81:248–50.
9. Bourlinos AB, Karakassides MA, Simopoulos A, Petridis D. Synthesis and characterization of magnetically modified clay composites. *Chem Mater.* 2000;12:2640–5.
10. Bourlinos AB, Devlin E, Boukos N, Simopoulos A, Petridis D. Magnetite and Co ferrite-based clay composites. *Clay Miner.* 2002;37:135–41.
11. Mastalir A, Notheisz F, Kiraly Z, Bartok M, Dekany I. Novel clay intercalated metal catalysts: a study of the hydrogenation of styrene and 1-octene on clay intercalated Pd catalysts. *Stud Surf Sci Catal.* 1997;108:477–84.
12. Penchev IP, Hristov JY. Behaviour of fluidized beds of ferromagnetic particles in an axial magnetic field. *Powder Technol.* 1990;61:103–18.
13. Yariv S. The role of charcoal on DTA curves of organo-clay complexes: an overview. *Appl Clay Sci.* 2004;24:225–36.
14. Morais LC, Valenzuela-Diaz FR, Dweck J, Büchler PM. Thermal analysis characterization of lactose and derived products in dairy product industry effluents processing. *J Therm Anal Calorim.* 2005;82:315–8.
15. Dweck J. Qualitative and quantitative characterization of Brazilian natural and organophilic clays by thermal analysis. *J Therm Anal Calorim.* 2008;92(1):129–35.
16. Lagaly G. Layer charge heterogeneity in vermiculites. *Clays Clay Miner.* 1982;30:215–22.
17. Jaynes WF, Boyd SA. Clay mineral type and organic compound sorption by hexadecyltrimethylammonium-exchanged clays. *Soil Sci Soc Am J.* 1991;55:43–8.
18. Cornell RM, Schwertmann U. The iron oxides. structure, properties, reactions, occurrences and uses. 1st ed. Weinheim: VCH; 1996. p. 127–73.
19. Tabak A, Afsin B, Aygun SF, Koksal E. Structural characteristics of organo-modified bentonites of different origin. *J Therm Anal Calorim.* 2007;87:375–81.
20. Chen D, Zhu JX, Yuan P, Yang SJ, Chen T-H, He HP. Preparation and characterization of anion-cation surfactants modified montmorillonite. *J Therm Anal Calorim.* 2008;94:841–8.